EVLA Memo #188
The Impact of the New Thermal Gap Receiver Assembly on the Sensitivity of the EVLA at C-Band (4–8 GHz)

Emmanuel Momjian (NRAO)

December 2, 2014

Abstract

Sensitivity measurements of the EVLA at C-band (4–8 GHz) are presented to assess the impact of the receivers with the new thermal gap assembly. The on-the-sky test results are consistent with lab measurements, and show sensitivity improvement across the full frequency range of the C-band receiver. The overall improvement in the sensitivity is ∼9.4%. In the frequency range 4–6 GHz, the sensitivity improves by an average value of ∼11.5%, while in the frequency range 6–8 GHz, the sensitivity improves by an average value of ∼7.3%. The largest improvement in sensitivity ($> 15\%$) is achieved in the frequency range 4.1–4.7 GHz.

1 Introduction

In 2010, a new thermal gap assembly was implemented on the C-band (4–8 GHz) receiver system of the EVLA. This implementation was initially used to assemble new C-band receivers for the VLBA antennas and replace their narrow-band C-band receivers between 2011 and 2012. In early 2012, and similar to the C-band receivers, a new thermal gap assembly was implemented on the L-band (1–2 GHz) receiver system of the EVLA. To date, 24 EVLA antennas are equipped with these new L-band receivers. Their impact on the sensitivity of L-band observations was presented in the EVLA Memo #165 (Momjian et al. 2012). In late 2013, the EVLA antennas have also started to be equipped with the C-band receivers that have the new thermal gap assembly.

Figure 1 shows a comparison of the receiver temperature between the old (*red*) and the new (*blue*) thermal gap assemblies of the EVLA C-band receiver system in RCP (*top*), in LCP (*middle*), and in the average of the two polarizations (*bottom*). These lab measurements show an overall improvement in the sensitivity across the full frequency range of the C-band, and a more significant improvement at its lowest frequencies between 4.0 and 4.8 GHz.

To quantify the improvement in the sensitivity due to the new thermal gap assembly of the C-band receivers in astronomical observations, on-the-sky test observations were carried out. During these observations a total of seven EVLA antennas were equipped with these new receivers.

2 Observations

The EVLA C-configuration observations at C-band were carried out on October 28, 2014, for a total of one hour. The calibrator source 3C147 (J0542+4951) and a nearby field devoid of strong continuum sources (hereafter "blank field") were observed in this session. The WIDAR correlator was configured to deliver three different frequency settings to cover the full frequency span of the C-band receiver with the 8-bit samplers. Sub-bands with bandwidths of 128 MHz and 128 spectral

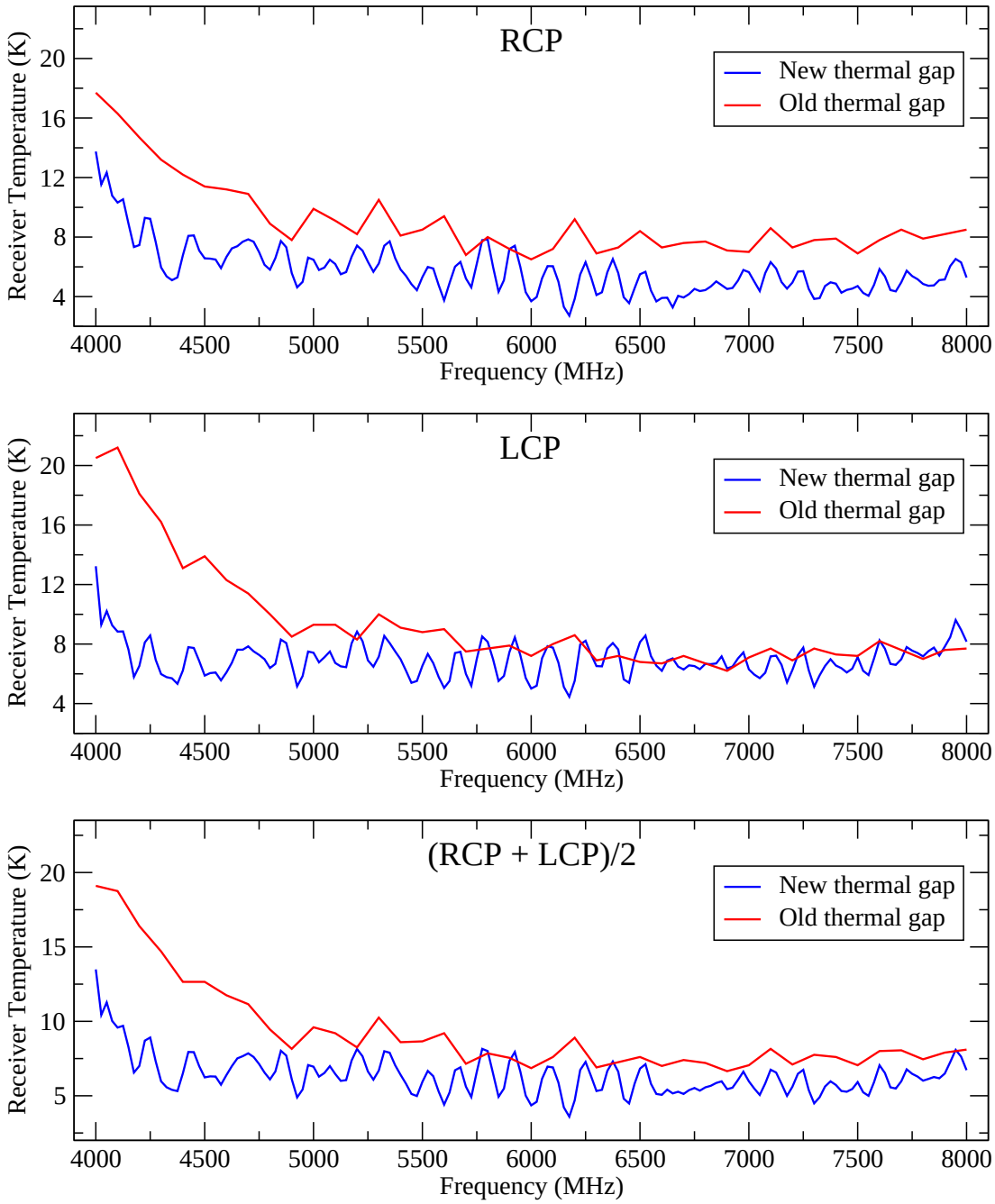

Figure 1: Lab measurements of the receiver temperature of an EVLA C-band receiver with the old (*red*) and another receiver with the new (*blue*) thermal gap assembly in the RCP (*top*), the LCP (*middle*), and the average of the two polarizations ([RCP + LCP]/2; *bottom*). The receiver temperature data are courtesy of W. Grammer and the front-end group of the VLA.

channels were used. The resulting spectral resolution was 1 MHz. The correlator integration time was set to 3 seconds. The frequencies of the three settings and of the baseband pairs in each setting were slightly overlapped to be able to exclude the noisier sub-band 0 data (EVLA Memo #154; Morris & Momjian 2012) from this sensitivity assessment without having any gaps in the frequency coverage. The frequency settings of the observations are listed in Table 1, and shown in Figure 2. In each setting, each baseband pair used 8 sub-bands that were contiguous in frequency, except in

the setting S3 where the baseband pair B0D0 used only two adjacent sub-bands, neither of which were sub-band 0.

Setup	Frequency Range (MHz)	
	Baseband Pair A0C0	Baseband Pair B0D0
S1	3672–4696	4546–5570
S2	5420–6444	6294–7318
S3	7168–8192	8170–8426

Table 1: Summary of the C-band (4–8 GHz) frequency settings. Frequencies below and above the nominal range of the receiver were included to assess the extended performance of the receiver.

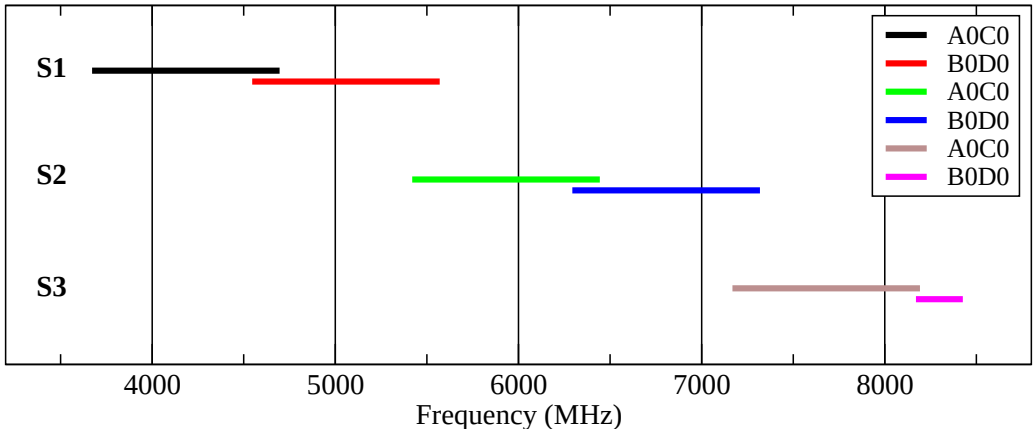

Figure 2: The three instrument configurations used for the C-band (4–8 GHz) observations. The indices (S1–S3) mark the individual settings and their respective baseband pairs and frequency ranges as listed in Table 1.

3 Data Reduction and Analysis

Data reduction and analysis were carried out in AIPS. The flux density scale was set using the Baars et al. 1977 coefficients for 3C147. After applying a priori flagging and excising integrations affected by interference, antenna based delay, complex gain and bandpass calibration solutions were obtained using the data of the calibrator source 3C147 for each sub-band and polarization product (i.e., RR and LL) separately. These solutions were then applied on the visibilities of the blank field, and spectra were generated to visually inspect its data in order to further ensure the exclusion of spectral channels that were affected by RFI from subsequent analysis.

Using the AIPS task UVHGM, the RMS noise values for Stokes I were measured by fitting Gaussian profiles on the histogram distributions of the blank field's real part of the visibilities. For this, channels from each sub-band that were not visibly contaminated by RFI were used. A 3-channel Hanning-smoothing was applied on the spectra in all the data reduction and analysis steps to reduce the Gibbs ringing phenomenon introduced by strong RFI features at various C-band frequencies.

Only seven of the EVLA antennas in the data set, namely ea01, ea06, ea11, ea16, ea19, ea23, and ea28, were equipped with the C-band receivers that have the new thermal gap assembly. The

sensitivity measurements reported in this memo are based on the average values of the baselines among these seven EVLA antennas. For comparison, sensitivity measurements were also obtained using the average values of all the baselines among the antennas that have the old thermal gap assembly.

As examples of the Gaussian noise in the data, Figure 3 shows histogram distributions of the blank field data using the visibilities of the baselines among all the antennas that have the C-band receivers with old thermal gap assembly (*top*), and among the seven antennas that have the C-band receivers with new thermal gap assembly (*bottom*), in two different sub-bands. Also shown are the resulting Gaussian profiles and parameters. The frequency on top of each plot denotes the value at the center of the continuous, RFI-free channel range used in each sub-band.

The RMS noise values obtained through the histogram fittings were then converted to System Equivalent Flux Densities (SEFDs) using the following equation:

$$\text{RMS (Jy)} = \frac{1}{2\eta_c\kappa_{hs}} \frac{\text{SEFD (Jy)}}{\sqrt{\beta\tau}}, \tag{1}$$

where β is the spectral channel width in Hz and τ is the correlator integration time in seconds ($\beta = 10^6$ Hz and $\tau = 3$ s in these data). η_c is the WIDAR correlator efficiency, and it is assumed to be 0.93 for the mode used in these observations, and κ_{hs} is the improvement in the signal-to-noise due to the application of the Hanning-smoothing, which is 1.633[1] for a 3-channel Hanning-smoothing.

For the EVLA, note that the SEFD is related to the system temperature ($T_{\rm sys}$) and the antenna illumination efficiency (A_e) by:

$$\text{SEFD (Jy)} = 5.62\ \frac{T_{\rm sys}\ \text{(K)}}{A_e}. \tag{2}$$

Multiple background continuum sources in the blank field contribute only a total of $S \sim 5$ mJy to the measurements at the lowest frequencies of C-band, and less than 1 mJy at the highest frequencies, as determined by imaging several of the sub-bands. However, no correction was performed in the RMS noise estimates to account for the background sources because even at the lowest frequencies of C-band their impact on the SEFD estimates is $\leq 0.5\%$.

4 Results and Discussion

Figure 4 shows the SEFD values in the EVLA C-band frequency range 4–8 GHz. The blue curve represents the average SEFD of the baselines among the seven antennas that have the C-band receivers with the new thermal gap assembly (ea01, ea06, ea11, ea16, ea19, ea23,and ea28). The red curve represents the average SEFD of the baselines among all the other antennas in the array that have the old C-band thermal gap assembly. The results show a clear improvement in the sensitivity across the full C-band frequency range. This is in very good agreement with the lab measurements (e.g., Figure 1–*bottom*).

Figure 5 shows the percentage change in the SEFD due to the new thermal gap assembly relative to the old thermal gap assembly. The positive values reflect lower SEFDs (i.e., improved sensitivity) due to the new thermal gap design.

As seen in Figure 5, and due to the new thermal gap assembly, the sensitivity is improved across the full range of the C-band frequency (4–8 GHz) by at least 3.6% and as much as 20.4%. The average improvement in the sensitivity across the full frequency range is ∼9.4%. In the frequency range 4–6 GHz, the sensitivity improves by an average value of ∼11.5%, while in the frequency

[1]The improvement in signal-to-noise due to a 3-channel Hanning-smoothing is $1/\sqrt{0.25^2 + 0.5^2 + 0.25^2}$=1.633

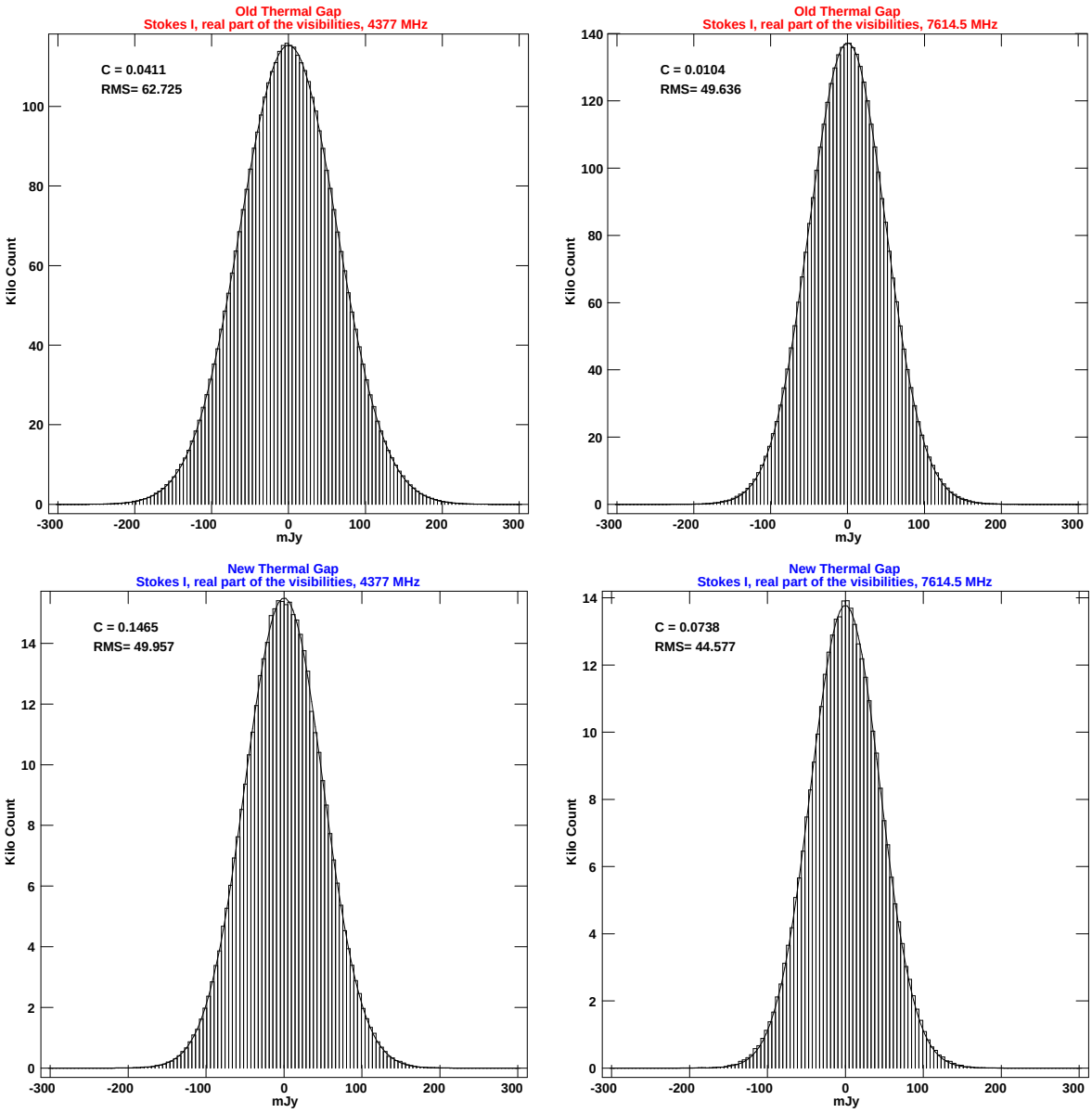

Figure 3: Histogram distributions of the blank field data of the baselines among all the antennas that have C-band receivers with the old thermal gap assembly (*top*), and among the seven antennas that have the C-band receivers with new thermal gap assembly (*bottom*), in two different sub-bands. Also shown are the fitted Gaussian profiles. A continuous, RFI-free channel range per sub-band, Stokes I, and the real part of the visibilities were used to make these histograms and measure the RMS noise.

range 6–8 GHz, the sensitivity improves by an average value of ∼7.3%. The largest improvement in sensitivity ($> 15\%$) is achieved in the frequency range 4.1–4.7 GHz, with the peak sensitivity improvement (∼20%) being near 4.3 GHz.

Contrary to the lab measurements presented in Figure 1, where the receiver temperature of the new thermal gap receiver assembly is constant for most of the C-band frequency range, i.e., between 4.3 and 8.0 GHz, and rises at the lowest frequencies (4.0–4.3 GHz), the on-the-sky SEFD measurements (Figure 4) show a degradation in the sensitivity starting near 6.7 GHz and downwards

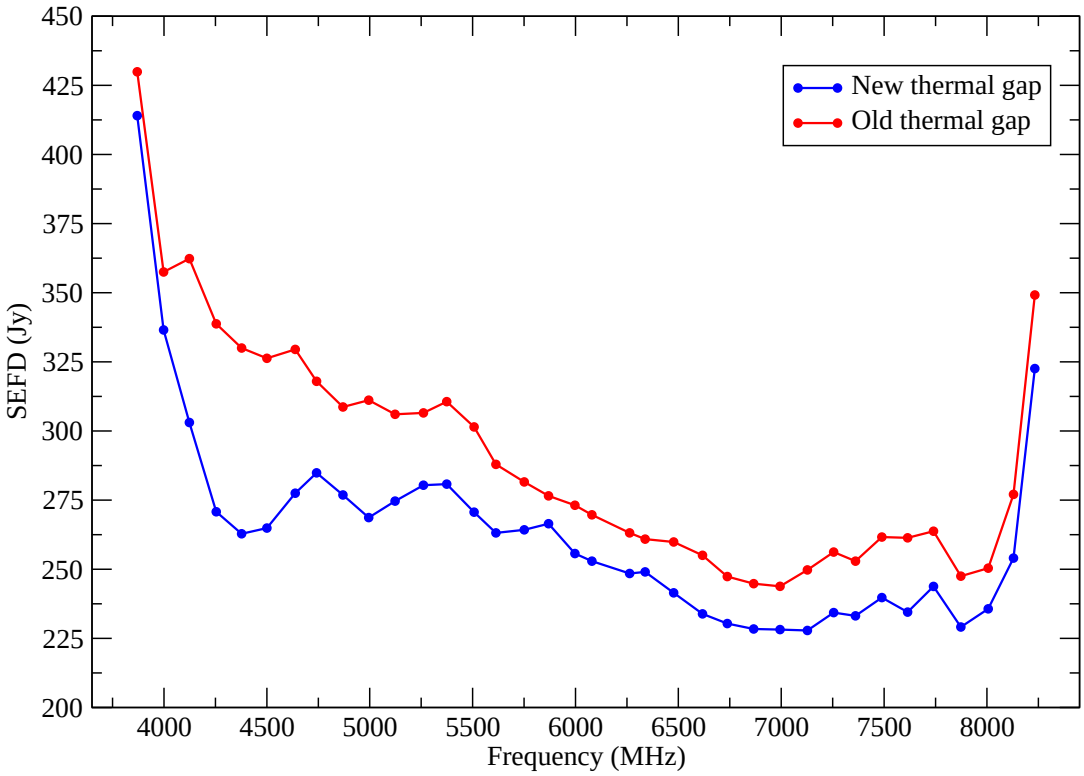

Figure 4: The SEFD values in the EVLA C-band frequency range 4–8 GHz. The blue curve represents the average SEFD of the baselines among the seven antennas that have the C-band receivers with the new thermal gap assembly (ea01, ea06, ea11, ea16, ea19, ea23,and ea28). The red curve represents the average SEFD of the baselines among all the other antennas that have the old C-band thermal gap assembly.

in frequency. This loss in sensitivity is most likely caused by a drop in the antenna efficiency, whose origin presumably lies in the feed horn illumination pattern.

As noted in Table 1, the on-the-sky observations included frequency tunings that are outside the nominal range of C-band (4–8 GHz). Even though it is possible to tune the C-band receivers down to 3672 MHz and up to 8426 MHz, a significant loss in sensitivity is seen below 3850 MHz and above 8250 MHz as shown in Figure 6. Therefore, observations below and above these noted frequencies using the C-band receivers should be avoided.

Overall, the on-the-sky test results show a net sensitivity improvement that should benefit continuum observations which require the full C-band frequency range. Moreover, this clear sensitivity improvement will be of importance to various spectral line observations such as vibrational HCN, excited OH, methanol, formaldehyde, and various radio recombination lines that fall within the frequency span of the C-band receiver.

5 Acknowledgements

The author would like to thank W. Grammer for providing the lab measurements of the receiver temperature, and R. Perley for helpful comments and discussions.

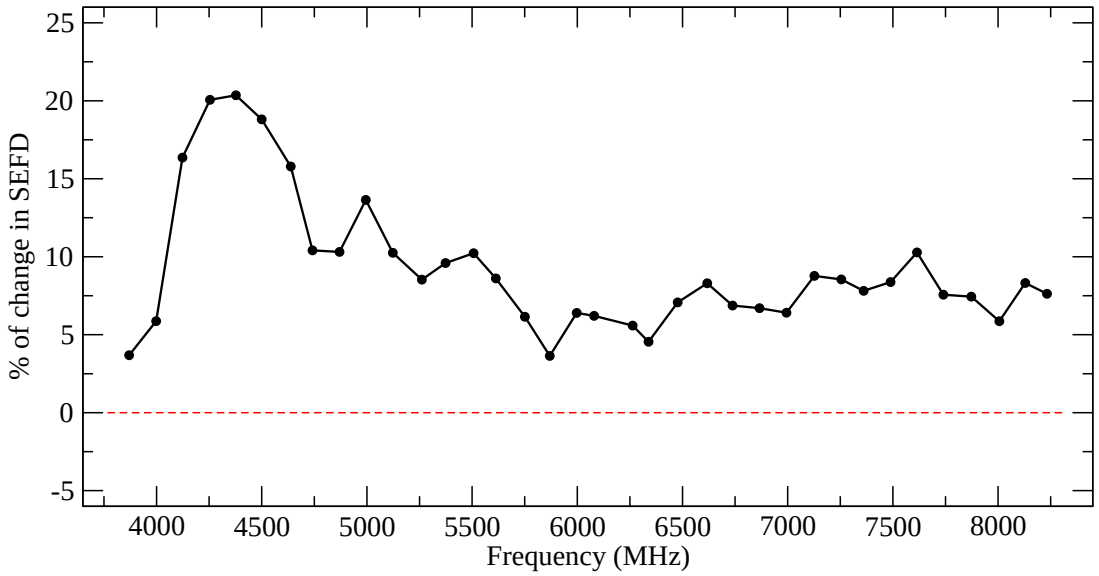

Figure 5: The percentage change in the SEFD due to the new thermal gap assembly relative to the old thermal gap assembly. Positive values reflect lower SEFDs (i.e., improved sensitivity) due to the new thermal gap design.

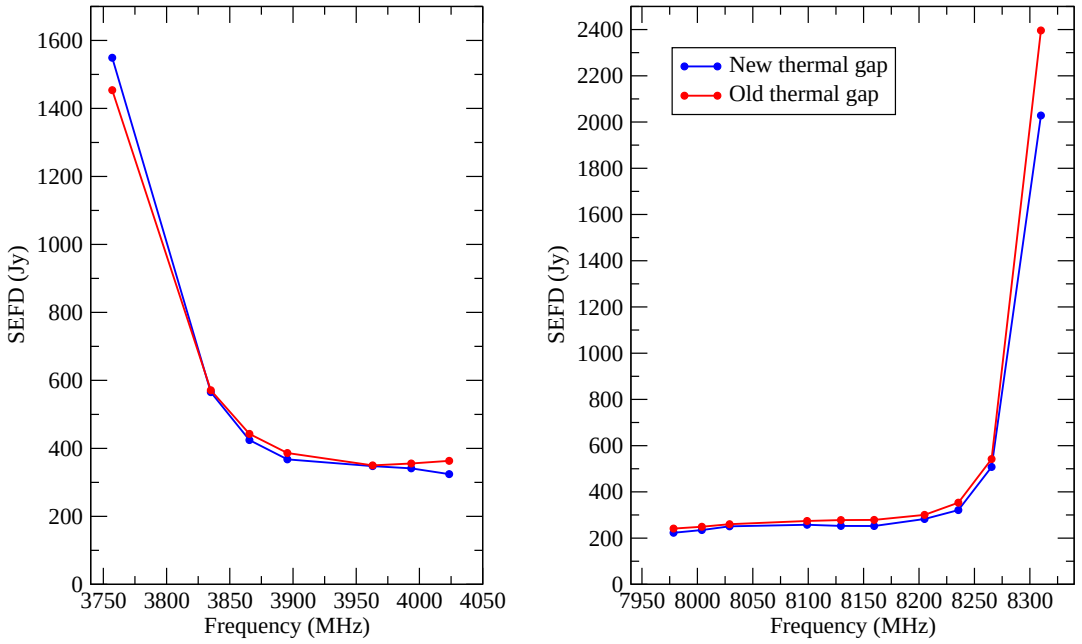

Figure 6: The SEFD values below (*left*) and above (*right*) the nominal frequency range of the EVLA C-band (4–8 GHz) receiver. In both panels the blue curve represents the average SEFD of the baselines among the seven antennas that have the C-band receivers with the new thermal gap assembly, and the red curve represents the average SEFD of the baselines among all the other antennas that have the old C-band thermal gap assembly. A significant loss in sensitivity can be seen below 3850 MHz and above 8250 MHz. Observations below and above these frequencies using the C-band receivers should be avoided.